Journal of Materials Chemistry C

PAPER

View Article Online
View Journal | View Issue

Cite this: J. Mater. Chem. C, 2017, 5, 3623

Magnetostructural correlations in $BiFeO_3$-based multiferroics

V. A. Khomchenko, *[a] D. V. Karpinsky[b] and J. A. Paixão[a]

Received 23rd February 2017,
Accepted 17th March 2017

DOI: 10.1039/c7tc00833c

rsc.li/materials-c

Inspired by the potential applications of the magnetoelectric effect, interest in multiferroic materials is growing steadily. While $BiFeO_3$ is the most thoroughly studied magnetic ferroelectric compound, the properties of its solid solutions remain a matter of intensive debate. In this paper we show how variation in the chemical composition of $Bi_{1-x}Ae_xFe_{1-x}Ti_xO_3$ (Ae = Ca, Sr, Ba) perovskites affects their crystal structure and magnetic behavior. In particular, our research demonstrates that Ca/Ti and Sr/Ti substitutions suppress the cycloidal antiferromagnetic structure specific to the parent compound, thus stabilizing a weak ferromagnetic ferroelectric state. The Ba/Ti-doped solid solutions retain the magnetic behavior characteristic of the pure $BiFeO_3$. Since the latter observation is directly opposed to the prevailing concept used in describing magnetic phenomena in the $Bi_{1-x}Ba_xFe_{1-x}Ti_xO_3$ series, the origin of the contradiction between the current and previously reported data is analyzed. Finally, the reasons underlying the difference in the magnetic properties of the $Bi_{1-x}Ae_xFe_{1-x}Ti_xO_3$ compounds are discussed.

1. Introduction

Magnetoelectric multiferroics exhibit the simultaneous existence of spin and electric dipole ordering, making them promising for future technological applications.[1] An ideal multiferroic material is expected to be ferromagnetic and ferroelectric, and demonstrate strong coupling between magnetization and polarization at room temperature. Since such a material has not been discovered so far, much attention now focuses on the antiferromagnetic (AFM) and ferroelectric (FE) bismuth iron oxide,[2,3] which possesses exceptionally high transition temperatures ($T_{AFM} \approx 640$ K, $T_{FE} \approx 1100$ K) and very large spontaneous polarization ($P_s \sim 100$ μC cm^{-2}). Pure $BiFeO_3$ is a perovskite with a rhombohedral crystal lattice (space group *R3c*)[4] and cycloidal spin arrangement[5] stable over a broad range of magnetic fields.[6] Both the crystal and magnetic structures can be influenced by the chemical replacement of Bi^{3+} with rare-earth (Re) or alkali-earth (Ae) elements.[7–9] Depending on the concentration and ionic radius of the Re^{3+} cations, either the antipolar (generally, $PbZrO_3$-related) or nonpolar $GdFeO_3$-type structure can be stabilized.[10–14] The doping-driven loss of the ferroelectric ordering is accompanied by the removal of the cycloidal magnetic modulation resulting in the appearance of a small (~0.25–0.3 emu g^{-1}) spontaneous magnetization originating from the canting of the antiferromagnetic sublattices (the Heisenberg nearest-neighbor exchange establishes a G-type AFM structure) induced by the Dzyaloshinskii–Moriya interaction.[11–13] In contrast to the $Bi_{1-x}Re_xFeO_3$ multiferroics, the $Bi_{1-x}Ca_xFeO_{3-x/2}$ perovskites can exhibit a purely weak ferromagnetic (wFM) behavior in the polar phase,[15] thus providing the technologically important possibility of switching the ferroelectric polarization with a magnetic field. The origin of the Ca^{2+} substitution-driven instability of the cycloidal order has been shown to be closely connected with the charge-compensatory mechanism that involves the formation of anion vacancies in the acceptor-doped materials.[16–18] Nevertheless, the doping-introduced lattice defects seem not to be the only factor determining the evolution of magnetic properties in the $Bi_{1-x}Ae_xFeO_{3-x/2}$ series. Indeed, the $Bi_{1-x}Ba_xFeO_{3-x/2}$ ferroelectrics have been proven to be antiferromagnetic, thus suggesting that the size of an alkali-earth substituent should also play an important role.[19] The influence of the size of the Ae^{2+} cations could be more fully understood by considering the multiferroic behavior of the $Bi_{1-x}Ae_xFe_{1-x}Ti_xO_3$ perovskites. Unfortunately, the available data do not always provide a clear picture of how the variation in the ionic radius of Ae^{2+} affects the magnetic properties of the co-doped $BiFeO_3$. For instance, it is widely accepted that the $Bi_{1-x}Ba_xFe_{1-x}Ti_xO_3$ solid solutions are intrinsically weakly ferromagnetic.[20–25] It is assumed that the room-temperature spontaneous magnetization remains observable in a very broad concentration range.[21–25] Being based on a magnetometric study, these conclusions, however, are not consistent with the results of Mössbauer spectroscopy which indicate that some of these "weak ferromagnets" are in a magnetically-disordered state.[21,22] The existing magnetic data do not reveal any qualitative or quantitative similarities in the

[a] CFisUC, Department of Physics, University of Coimbra, P-3004-516 Coimbra, Portugal. E-mail: uladzimir@fis.uc.pt; Fax: +351 239 829 158; Tel: +351 239 410 637

[b] Scientific-Practical Materials Research Centre of NAS of Belarus, 220072 Minsk, Belarus

compositional dependences of the spontaneous magnetization,[21–25] thus raising the question as to whether they can adequately reflect the substitution-driven changes in the magnetic structure of the $Bi_{1-x}Ba_xFe_{1-x}Ti_xO_3$ compounds. Though the results of the magnetization measurements collected for the $Bi_{1-x}Sr_xFe_{1-x}Ti_xO_3$[26–30] and $Bi_{1-x}Ca_xFe_{1-x}Ti_xO_3$[19,31–33] systems look less contradictory, they are still not sufficiently consistent to describe the peculiarities of the antiferromagnetic–weak ferromagnetic transformation which supposedly takes place with increasing Ae^{2+}/Ti^{4+} content. To reveal the pattern of changes in the magnetic behavior of the co-doped bismuth ferrites depending on the concentration and ionic radius of the alkali-earth substituents, solid state synthesis and investigation of the crystal structure, microstructure, and local ferroelectric and magnetic properties of the $Bi_{1-x}Ae_xFe_{1-x}Ti_xO_3$ (Ae = Ca, Sr, Ba; $0.1 \leq x \leq 0.2$) perovskites have been carried out (due to the difference in their size, the Ae dopants were expected to provide dissimilar "chemical pressures" unequally affecting the stability of the cycloidal phase; the concentration range, in turn, was chosen as illustrating the mechanism of the anticipated composition-driven AFM–wFM transformation).[19–33]

2. Experimental

Ceramic samples of $Bi_{1-x}Ae_xFe_{1-x}Ti_xO_3$ (Ae = Ca, Sr, Ba; $0.1 \leq x \leq 0.2$) were prepared by a solid-state reaction method using high-purity powders of Bi_2O_3, $CaCO_3$, $SrCO_3$, $BaCO_3$, Fe_2O_3 and TiO_2 (Sigma-Aldrich, ≥99%). The reagents were taken in a stoichiometric cation ratio and mixed using an agate mortar and a pestle. The mixtures were uniaxially pressed into pellets with a diameter of 10 mm and a thickness of 2–3 mm and annealed in closed alumina crucibles at the temperatures specified in Table 1 (in all cases, the heating/cooling rate was 5 °C per min, and the duration of the heat treatment was 30 h). Phase and structure analyses were performed on crushed pellets using a Bruker D8 Advance diffractometer with Cu K_α radiation. The X-ray diffraction (XRD) patterns were collected by step scanning in the angle range $15^\circ \leq 2\theta \leq 100^\circ$ with a step of 0.01° and a dwell of 2 s per step. The diffraction data were analyzed by the Le Bail method[34] using the FullProf software package.[35] Microstructural and elemental analyses were done on gold–palladium coated ceramic surfaces using a VEGA-3 SB (TESCAN) scanning electron microscope (SEM) operating at an accelerating voltage of 30 kV and equipped with an energy dispersive X-ray spectroscopy (EDS) detector (Bruker). The ferroelectric domain structure was investigated with a NTEGRA Prima (NT-MDT) scanning probe microscope operating in piezoresponse force microscopy (PFM) mode (the NSG30 probes were used). Images of ferroelectric domains were recorded under an applied AC voltage with an amplitude $V_{AC} = 5$ V and a frequency $f = 100$ kHz. Magnetic measurements of ceramic samples were performed with a cryogen-free Physical Properties Measurement System (PPMS DynaCool, Quantum Design).

Table 1 Synthesis temperature and unit cell parameters (the accuracy is better than 0.0005 Å) for the $Bi_{1-x}Ae_xFe_{1-x}Ti_xO_3$ samples

Composition	T_{syn}, °C	a, Å	c, Å
$Bi_{0.9}Ca_{0.1}Fe_{0.9}Ti_{0.1}O_3$	920	5.5635	13.8138
$Bi_{0.85}Ca_{0.15}Fe_{0.85}Ti_{0.15}O_3$	940	5.5563	13.7859
$Bi_{0.8}Ca_{0.2}Fe_{0.8}Ti_{0.2}O_3$	960	5.5495	13.7527
$Bi_{0.9}Sr_{0.1}Fe_{0.9}Ti_{0.1}O_3$	920	5.5774	13.8324
$Bi_{0.88}Sr_{0.12}Fe_{0.88}Ti_{0.12}O_3$	930	5.5777	13.8210
$Bi_{0.85}Sr_{0.15}Fe_{0.85}Ti_{0.15}O_3$	940	5.5778	13.7978
$Bi_{0.8}Sr_{0.2}Fe_{0.8}Ti_{0.2}O_3$	960	5.5778	13.7654
$Bi_{0.9}Ba_{0.1}Fe_{0.9}Ti_{0.1}O_3$	910	5.5950	13.8875
$Bi_{0.85}Ba_{0.15}Fe_{0.85}Ti_{0.15}O_3$	920	5.6044	13.8883
$Bi_{0.8}Ba_{0.2}Fe_{0.8}Ti_{0.2}O_3$	930	5.6152	13.8874

3. Results and discussion

XRD measurements confirmed the as-prepared samples (Table 1) to be single phase and having the rhombohedral lattice characteristic of the parent $BiFeO_3$.[4] Indeed, all the collected diffraction patterns were successfully indexed using the hexagonal cell with $a = \sqrt{2}a_p$ and $c = 2\sqrt{3}c_p$ ($a_p \approx c_p \sim 4$ Å are the parameters of the primitive pseudocubic perovskite subcell; the unit cell, accordingly, contains 6 formula units) to yield the systematic absence of the reflections indicative of the space group $R3c$. The results are consistent with the majority of the previously published data reported on the crystal structure of the $Bi_{1-x}Ae_xFe_{1-x}Ti_xO_3$ compounds at $x \leq 0.2$.[19–21,23–29,31,32] A typical example of the refined XRD pattern is shown in Fig. 1. The unit cell parameters obtained from the Le Bail fits are summarized in Table 1.

The changes observed in the lattice parameters of the $Bi_{1-x}Ae_xFe_{1-x}Ti_xO_3$ samples with increasing x are largely determined by the ionic radius (r) of the Ae^{2+} ions ($r_{Ca^{2+}} < r_{Bi^{3+}} < r_{Sr^{2+}} < r_{Ba^{2+}}$, $r_{Ti^{4+}} < r_{Fe^{3+}}$).[36] An increase in the concentration of Ca^{2+} and Ti^{4+} gives rise to a contraction of the cell both in the basal hexagonal plane and along the polar c direction (Fig. 2(a)). Though the size of Sr^{2+} exceeds that of Bi^{3+},[36] the common effect of Sr^{2+}/Ti^{4+} co-doping is a decrease of the primitive cell volume (Fig. 2(b)) associated with a contraction of the crystal lattice along the polar c axis (Fig. 2(a)). Increasing the content of Ba^{2+} and Ti^{4+} causes a lattice expansion in the basal ab plane,

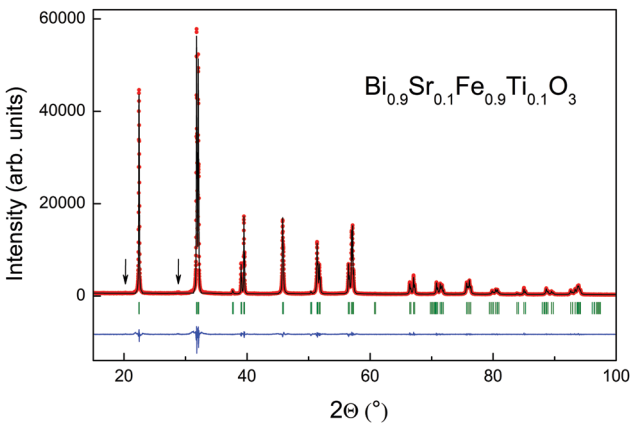

Fig. 1 Experimental (red circles), calculated (black line) and difference (blue line) XRD patterns obtained for the $Bi_{0.9}Sr_{0.1}Fe_{0.9}Ti_{0.1}O_3$ compound. Tick marks indicate the positions of allowed Bragg reflections. The peaks seen at around 20° and 29° (marked by arrows) are due to the small K_β component of the radiation leaking through the K_β filter.

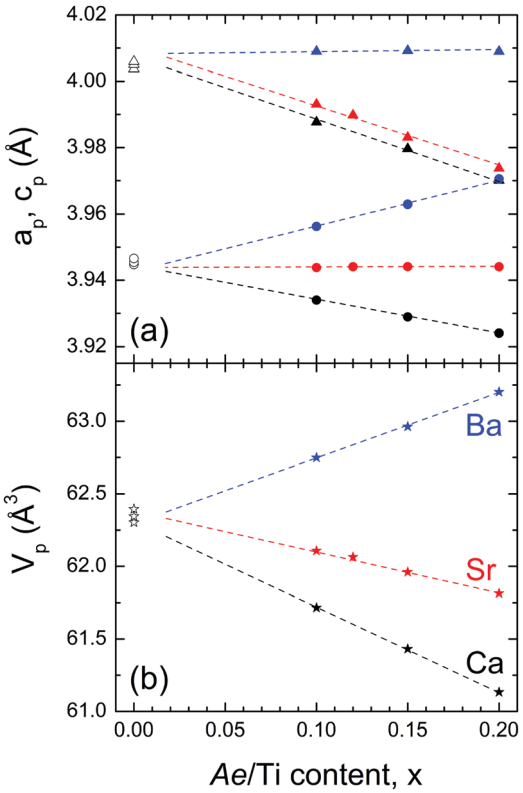

Fig. 2 (a) Normalized lattice parameters a_p and c_p (depicted as circles and triangles, respectively) for the $Bi_{1-x}Ae_xFe_{1-x}Ti_xO_3$ [Ae = Ca (black symbols), Sr (red symbols), Ba (blue symbols)] compounds. (b) Primitive cell volume for the $Bi_{1-x}Ae_xFe_{1-x}Ti_xO_3$ samples. The data for pure $BiFeO_3$ (white symbols) were taken from ref. 37–39. The lines are guides for the eye.

while the c parameter remains nearly constant and, thus, quite similar to that specific to the pure $BiFeO_3$ (Fig. 2(a)).

The pattern of changes in the magnetic behavior of the $Bi_{1-x}Ae_xFe_{1-x}Ti_xO_3$ compounds was found to be strongly dependent on the size of the Ae^{2+} substituents. The Ca/Ti co-doping results in the suppression of the cycloidal magnetic structure, as evident from the field dependences of magnetization shown in Fig. 3(a). The sample with $x = 0.1$ exhibits a metamagnetic transition associated with the field-induced removal of the cycloidal modulation and stabilization of a spin-canted antiferromagnetic order.[40] The deviation from a linear increase in magnetization that reflects the reversible cycloidal structure ↔ canted structure transformation is observed over the range 25–65 kOe (in the pure $BiFeO_3$, such a transition begins at $H \sim 160$ kOe and continues up to $H \sim 200$ kOe).[6] The $x = 0.15$ sample shows a metamagnetic behavior at much lower fields (the transformation starts immediately upon the application of a magnetic field, though the homogeneous spin-canted state is stabilized only at $H > 35$ kOe). A further increase in the concentration of Ca and Ti gives rise to spontaneous weak ferromagnetism (Fig. 3(a)).

Magnetic phase evolution in the $Bi_{1-x}Sr_xFe_{1-x}Ti_xO_3$ series can be characterized in terms of the formation of an intermediate inhomogeneous magnetic state. The canted and cycloidal phases coexist in a broad concentration range, as can be seen from the $M(H)$ dependences combining a relatively large remanent magnetization (up to 0.1 emu g^{-1} for $x = 0.15$) with a metamagnetic behavior (Fig. 3(b)). Though our investigations suggest that the magnetic properties of the samples are hardly affected by the annealing temperature (Fig. 4), we cannot rule out the possibility that the synthesis procedure can be optimized to yield the pronounced magnetic transitions specific to the Ca/Ti-doped compounds (Fig. 3(a)). The tendency towards magnetic phase separation is likely associated with a large difference in the ionic radii of the host and substituting ions which is known to hamper a random distribution of the elements in the crystal lattice of perovskite-type materials.[41,42]

The Ca/Ti- and Sr/Ti-containing series exhibit the same trend with respect to the behavior of magnetization in high fields: after completing the metamagnetic transformation, those samples with an antiferromagnetic component at $H = 0$ acquire magnetization characteristic of the weak ferromagnetic solid solutions with $x = 0.2$ (Fig. 3(a and b)). The latter indicates that the field-stabilized and spontaneously-stabilized weak ferromagnetic phases have the same magnetization and, therefore, the same canted magnetic structure, as predicted by the symmetry of the space group $R3c$ (if the Fe magnetic moments which form a G-type antiferromagnetic order are oriented perpendicular to the c axis, the symmetry permits a canting of the antiferromagnetic sublattices resulting in a weak ferromagnetism).[43] The difference

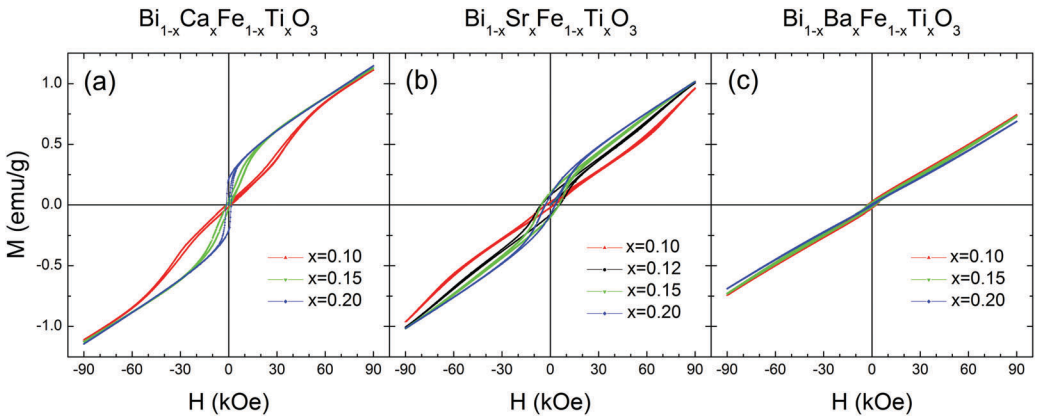

Fig. 3 Magnetic hysteresis loops obtained for the $Bi_{1-x}Ae_xFe_{1-x}Ti_xO_3$ compounds at room temperature.

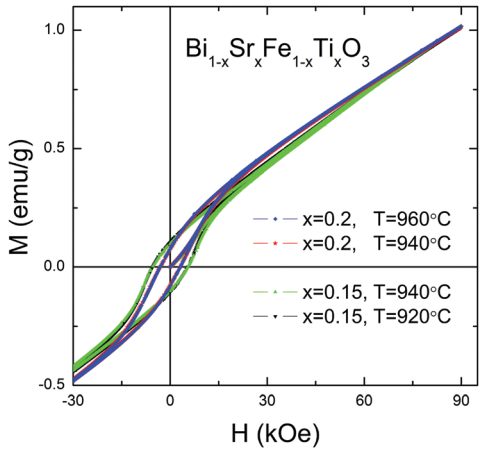

Fig. 4 Room-temperature magnetic hysteresis loops obtained for the $Bi_{1-x}Sr_xFe_{1-x}Ti_xO_3$ (x = 0.15, 0.2) samples prepared at different temperatures.

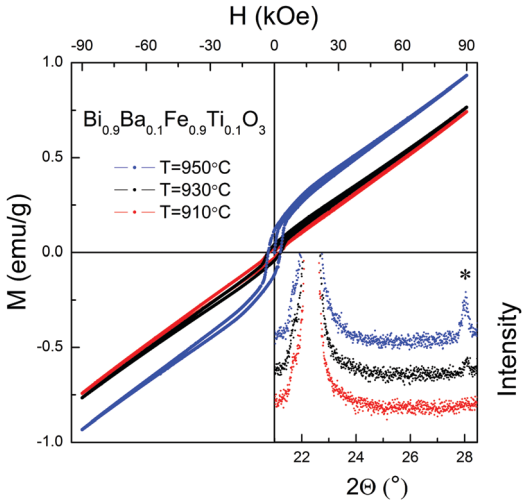

Fig. 5 Room-temperature magnetic hysteresis loops obtained for the $Bi_{0.9}Ba_{0.1}Fe_{0.9}Ti_{0.1}O_3$ samples prepared at different temperatures. The inset shows parts of the experimental XRD patterns collected for the same samples and demonstrating the appearance of extra peaks (marked by asterisk) attributable to the formation of $Bi_2Fe_4O_9$ impurities (intensity of the main impurity peak detected for the sample annealed at 950 °C is around 100 times smaller than that characteristic of the most intensive peaks originating from the perovskite phase).

in values of the spontaneous magnetization obtained for the Ca/Ti- and Sr/Ti-doped compounds with $x = 0.2$ ($M_s \approx 0.35$ emu g^{-1} for Ae = Ca and $M_s \approx 0.25$ emu g^{-1} for Ae = Sr, as defined from a linear extrapolation of the high field magnetization to $H = 0$) should be associated with a compositional variation in the amplitude of the oxygen octahedra rotation determining the magnitude of the spin canting in the weak ferromagnetic phase.[44]

In contrast to the majority of the available data,[20–25] our investigations show that the $Bi_{1-x}Ba_xFe_{1-x}Ti_xO_3$ solid solutions are antiferromagnetic, the apparent "weak ferromagnetism" being due to the presence of magnetic impurities. Indeed, magnetic measurements of the Ba/Ti-doped samples reveal almost perfectly linear $M(H)$ dependences with a negligible remanent magnetization (Fig. 3(c)). The magnetic behavior is easily affected by the synthesis conditions: an increase in the annealing temperature gives rise to an enhancement of the ferromagnetic-like contribution (Fig. 5). The magnetization increase is accompanied by the appearance of extra peaks in the XRD patterns (inset in Fig. 5). The peaks can be identified as originating from the $Bi_2Fe_4O_9$ impurity arising as a result of heat-induced decomposition of the perovskite phase.[45] Even though the detected impurity cannot be responsible for the increased magnetization ($Bi_2Fe_4O_9$ is paramagnetic at room temperature),[46] the correlation between the magnetic and XRD data (Fig. 5) implies that the magnetic state of the samples should be determined by their phase composition.

To reveal the origin of the spontaneous magnetization appearing in the partly decomposed samples, a combined SEM/EDS analysis has been carried out (Fig. 6 and 7). The $Bi_{0.8}Ca_{0.2}Fe_{0.8}Ti_{0.2}O_3$ and $Bi_{0.8}Ba_{0.2}Fe_{0.8}Ti_{0.2}O_3$ samples, selected as representing a purely weak ferromagnetic and antiferromagnetic material, respectively (Fig. 3(a and c)), showed no features in the SEM images that could be indicative of an elemental heterogeneity (Fig. 6). In contrast, backscattered electron microscopy, performed for the $Bi_{0.9}Ba_{0.1}Fe_{0.9}Ti_{0.1}O_3$ sample annealed at 950 °C (Fig. 5), revealed the presence of grains distinguished by elemental contrast. Among others, the grains enriched in Fe and depleted in Bi were detected (Fig. 7). The chemical composition of these grains

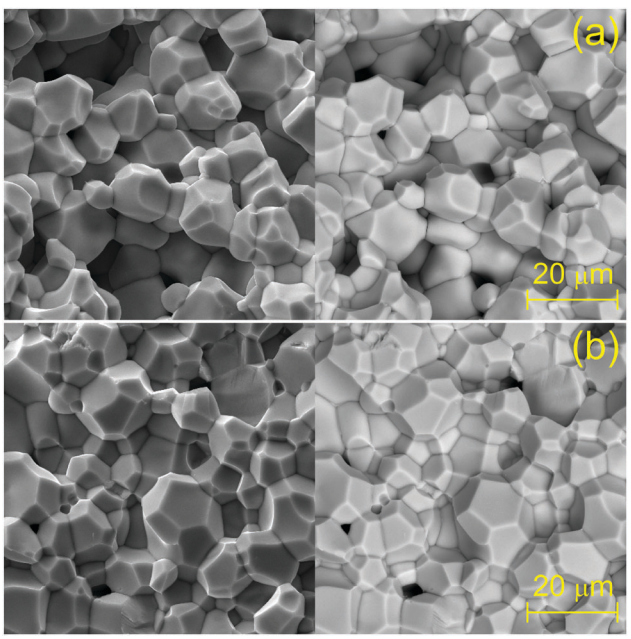

Fig. 6 Secondary electron (left) and backscattered electron (right) images of the $Bi_{0.8}Ca_{0.2}Fe_{0.8}Ti_{0.2}O_3$ (a) and $Bi_{0.8}Ba_{0.2}Fe_{0.8}Ti_{0.2}O_3$ (b) ceramics.

was found to correspond to the Ti-doped hexaferrite $BaFe_{12}O_{19}$. Taking into account that the coercive field specific to the chemically-inhomogeneous $Bi_{0.9}Ba_{0.1}Fe_{0.9}Ti_{0.1}O_3$ samples ($H_c \sim 3$ kOe) is very close to that characteristic of the $BaFe_{12}O_{19}$ ceramics[47] and $BaFe_{12}O_{19}$-containing composites,[48,49] the presence of the ferrimagnetic impurity should be considered as the most probable reason underlying the pseudo weak ferromagnetic behavior observed (Fig. 5). The results support the conclusions of the

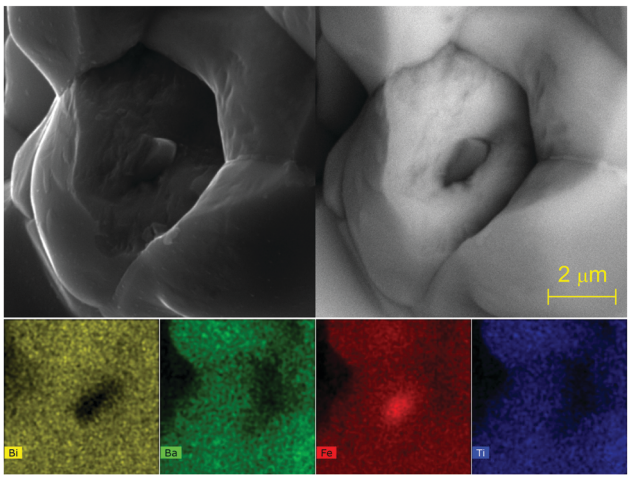

Fig. 7 Secondary electron image (left panel), backscattered electron image (right panel) and elemental maps (bottom panels) obtained for the $Bi_{0.9}Ba_{0.1}Fe_{0.9}Ti_{0.1}O_3$ sample annealed at 950 °C.

previous study of Clemens *et al.* indicating that the $BaFe_{12}O_{19}$ impurity phase gives rise to the apparent weak ferromagnetism in the $Bi_{1-x}Ba_xFeO_{3-x/2}$ and $Bi_{1-x}Ba_xFeO_{3-x}F_x$ compounds.[50] Being hardly detectable by XRD,[50] this impurity can seriously hamper the finding of real structure–property correlations, so a careful examination of the data reported on the multiferroic behavior of the $Bi_{1-x}Ba_xFe_{1-x}Ti_xO_3$ perovskites is highly desirable.

It has been recently shown that the magnetic properties of $BiFeO_3$-based multiferroics can be influenced by structural defects.[16–18,51–53] Indeed, even a small deviation from the ideal cation–anion stoichiometry that results in the appearance of lattice defects can trigger the removal of the cycloidal magnetic order, thus giving rise to a weak ferromagnetic behavior.[54] Taking into consideration that the distribution/concentration of the defects affects the ferroelectric domain structure of a material,[55] a PFM study aimed at revealing any possible correlations between the microstructure and magnetic properties has been performed (typical PFM images obtained for the weak ferromagnetic sample $Bi_{0.8}Ca_{0.2}Fe_{0.8}Ti_{0.2}O_3$ and antiferromagnetic sample $Bi_{0.8}Ba_{0.2}Fe_{0.8}Ti_{0.2}O_3$ are shown in Fig. 8; other data describing the compositional evolution of the domain structure in the $Bi_{1-x}Ca_xFe_{1-x}Ti_xO_3$ series have been recently presented in ref. 56). One can see that the samples demonstrate very similar ferroelectric/ferroelastic[4] domain patterns imprinting distribution of lattice defects which pin the domain walls.[18,55] Such a similarity does not conform to the scenario of the defect-driven suppression of cycloidal magnetic structure suggesting that the change of the magnetic state should be accompanied by dramatic morphological transformations giving rise to the appearance of nanoscale polarization textures.[16–18,52–54,57,58]

The magnetic structure of $BiFeO_3$ is stabilized by the antisymmetric Dzyaloshinskii–Moriya (DM) interaction of the form $E_{DM} = \sum_{ij} \mathbf{D}_{ij} \cdot (\mathbf{S}_i \times \mathbf{S}_j)$, where the DM vector, **D**, has two components associated with the ferroelectric polarization and with the antiphase rotations of FeO_6 octahedra.[59] It is assumed that if the DM energy associated with the octahedral rotations

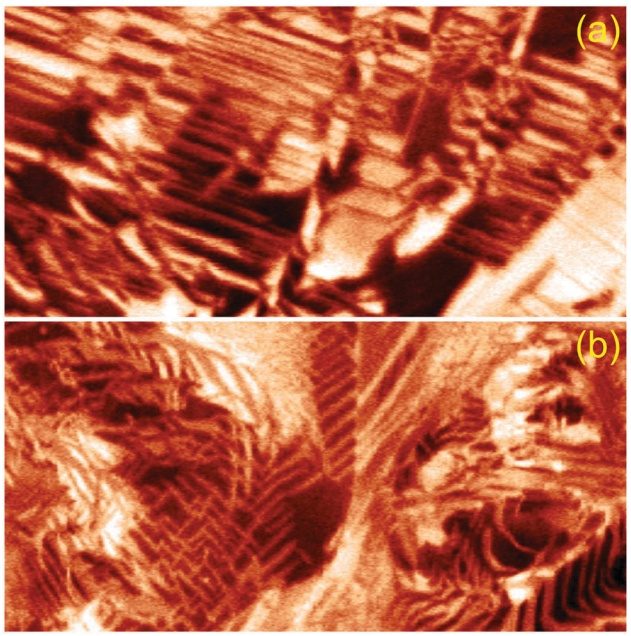

Fig. 8 Vertical PFM images (10 × 5 μm) of the mechanically-polished ceramics of $Bi_{0.8}Ca_{0.2}Fe_{0.8}Ti_{0.2}O_3$ (a) and $Bi_{0.8}Ba_{0.2}Fe_{0.8}Ti_{0.2}O_3$ (b). Domains with different orientation of polarization are distinguished by different contrast.

becomes larger than that of the ferroelectric polarization, the cycloidal state is destabilized in favour of a G-type structure with a net ferromagnetic component induced by spin canting in the basal plane.[59] Chemical substitution can affect both the magnitude of the oxygen octahedra rotations and the average polarizability of the A-site cations, thus becoming a tool for tuning the multiferroic behavior. Even though the laboratory XRD experiment does not permit a precise pattern of the composition-driven changes in the crystal structure of the $Bi_{1-x}Ae_xFe_{1-x}Ti_xO_3$ compounds to be obtained, it reveals the magneto-structural correlations (Fig. 2 and 3) consistent with the conception proposed. Indeed, one can see that the weak ferromagnetic state is attained only in those series in which the substitution gives rise to an anisotropic contraction of the cell along the polar *c* axis (such a contraction reflects the diminishing of polar ionic displacements[60,61]). The $Bi_{1-x}Ba_xFe_{1-x}Ti_xO_3$ (x = 0.1, 0.15, 0.2) compounds, in turn, exhibit composition-independent magnetic behavior (Fig. 3(c)) coinciding with that specific to the pure $BiFeO_3$.[12] The remarkable independence of the magnetic properties on the chemical composition correlates with the structural data suggesting a negligible variation in the *c* parameter over the concentration range under study (Fig. 2(a)).

4. Conclusions

The magnetic properties of the $Bi_{1-x}Ae_xFe_{1-x}Ti_xO_3$ (Ae = Ca, Sr, Ba) multiferroics have been studied as a function of the concentration and ionic radius of the alkali-earth substituents. It has been found that the Ca/Ti and Sr/Ti co-doping effectively modifies the magnetic structure of $BiFeO_3$, thus giving rise to the AFM–wFM transformation occurring without a change in

the crystal symmetry. Contrary to the mainstream view on the magnetic behavior of the $Bi_{1-x}Ba_xFe_{1-x}Ti_xO_3$ perovskites,[20–25] our investigations reveal that the materials retain the AFM state characteristic of the pure bismuth ferrite. We propose that the apparent weak ferromagnetism which can be seen in the Ba/Ti-doped samples should be associated with a deviation from nominal stoichiometric composition accompanied by the formation of magnetic impurities. The composition-driven changes in the magnetic properties of the $Bi_{1-x}Ae_xFe_{1-x}Ti_xO_3$ solid solutions correlate with the evolution of lattice parameters, thus confirming the existence of a tight coupling between the magnetic and structural/electric dipole order in these materials.

Acknowledgements

This work was supported by funds from FEDER (Programa Operacional Factores de Competitividade COMPETE) and from FCT-Fundação para a Ciência e a Tecnologia under the project UID/FIS/04564/2016. V. A. K. is grateful to Fundação para a Ciência e a Tecnologia for financial support through the FCT Investigator Programme (project IF/00819/2014). D. V. K. is grateful to BRFFR (grant F16R-066). Access to the TAIL-UC facility funded under QREN-Mais Centro project ICT_2009_02_012_1890 is gratefully acknowledged.

References

1 M. M. Vopson, *Crit. Rev. Solid State Mater. Sci.*, 2015, **40**, 223–250.
2 G. Catalan and J. F. Scott, *Adv. Mater.*, 2009, **21**, 2463–2485.
3 D. Sando, A. Barthélémy and M. Bibes, *J. Phys.: Condens. Matter*, 2014, **26**, 473201.
4 F. Kubel and H. Schmid, *Acta Crystallogr., Sect. B: Struct. Sci.*, 1990, **46**, 698–702.
5 R. D. Johnson, P. Barone, A. Bombardi, R. J. Bean, S. Picozzi, P. G. Radaelli, Y. S. Oh, S.-W. Cheong and L. C. Chapon, *Phys. Rev. Lett.*, 2013, **110**, 217206.
6 A. M. Kadomtseva, Yu. F. Popov, A. P. Pyatakov, G. P. Vorob'ev, A. K. Zvezdin and D. Viehland, *Phase Transitions*, 2006, **79**, 1019–1042.
7 C.-H. Yang, D. Kan, I. Takeuchi, V. Nagarajan and J. Seidel, *Phys. Chem. Chem. Phys.*, 2012, **14**, 15953–15962.
8 D. C. Arnold, *IEEE Trans. Ultrason. Ferroelectr. Freq. Control*, 2015, **62**, 62–82.
9 J. Wu, Z. Fan, D. Xiao, J. Zhu and J. Wang, *Prog. Mater. Sci.*, 2016, **84**, 335–402.
10 D. A. Rusakov, A. M. Abakumov, K. Yamaura, A. A. Belik, G. Van Tendeloo and E. Takayama-Muromachi, *Chem. Mater.*, 2011, **23**, 285–292.
11 I. O. Troyanchuk, D. V. Karpinsky, M. V. Bushinsky, V. A. Khomchenko, G. N. Kakazei, J. P. Araujo, M. Tovar, V. Sikolenko, V. Efimov and A. L. Kholkin, *Phys. Rev. B: Condens. Matter Mater. Phys.*, 2011, **83**, 054109.
12 V. A. Khomchenko, I. O. Troyanchuk, D. V. Karpinsky and J. A. Paixão, *J. Mater. Sci.*, 2012, **47**, 1578–1581.
13 I. Levin, M. G. Tucker, H. Wu, V. Provenzano, C. L. Dennis, S. Karimi, T. Comyn, T. Stevenson, R. I. Smith and I. M. Reaney, *Chem. Mater.*, 2011, **23**, 2166–2175.
14 V. A. Khomchenko, I. O. Troyanchuk, M. V. Bushinsky, O. S. Mantytskaya, V. Sikolenko and J. A. Paixão, *Mater. Lett.*, 2011, **65**, 1970–1972.
15 V. A. Khomchenko, I. O. Troyanchuk, D. M. Többens, V. Sikolenko and J. A. Paixão, *J. Phys.: Condens. Matter*, 2013, **25**, 135902.
16 V. A. Khomchenko and J. A. Paixão, *J. Appl. Phys.*, 2014, **116**, 214105.
17 V. A. Khomchenko, L. C. J. Pereira and J. A. Paixão, *J. Mater. Sci.*, 2015, **50**, 1740–1745.
18 V. A. Khomchenko and J. A. Paixão, *J. Phys.: Condens. Matter*, 2015, **27**, 436002.
19 I. O. Troyanchuk, M. V. Bushinsky, N. V. Tereshko and M. I. Kovetskaya, *JETP Lett.*, 2011, **93**, 512–516.
20 A. Singh, V. Pandey, R. K. Kotnala and D. Pandey, *Phys. Rev. Lett.*, 2008, **101**, 247602.
21 T.-J. Park, G. C. Papaefthymiou, A. J. Viescas, Y. Lee, H. Zhou and S. S. Wong, *Phys. Rev. B: Condens. Matter Mater. Phys.*, 2010, **82**, 024431.
22 R. A. M. Gotardo, D. S. F. Viana, M. Olzon-Dionysio, S. D. Souza, D. Garcia, J. A. Eiras, M. F. S. Alves, L. F. Cótica, I. A. Santos and A. A. Coelho, *J. Appl. Phys.*, 2012, **112**, 104112.
23 A. Singh, A. Senyshyn, H. Fuess, S. J. Kennedy and D. Pandey, *Phys. Rev. B: Condens. Matter Mater. Phys.*, 2014, **89**, 024108.
24 M. Kumar, S. Shankar, O. P. Thakur and A. K. Ghosh, *J. Mater. Sci.: Mater. Electron.*, 2015, **26**, 1427–1434.
25 H. Y. Dai, J. Chen, T. Li, D. W. Liu, R. Z. Xue, H. W. Xiang and Z. P. Chen, *J. Mater. Sci.: Mater. Electron.*, 2015, **26**, 3717–3721.
26 A. Y. Kim, S. H. Han, J. S. Kim and C. I. Cheon, *J. Korean Ceram. Soc.*, 2011, **48**, 307–311.
27 Z. Z. Ma, Z. M. Tian, J. Q. Li, C. H. Wang, S. X. Huo, H. N. Duan and S. L. Yuan, *Solid State Sci.*, 2011, **13**, 2196–2200.
28 D. J. Goossens, C. J. Weekes, M. Avdeev and W. D. Hutchison, *J. Solid State Chem.*, 2013, **207**, 111–116.
29 S. Vura, P. S. A. Kumar, A. Senyshyn and R. Ranjan, *J. Magn. Magn. Mater.*, 2014, **365**, 76–82.
30 H. Liu and X. Yang, *Ferroelectrics*, 2016, **500**, 310–317.
31 D. V. Karpinsky, I. O. Troyanchuk, J. V. Vidal, N. A. Sobolev and A. L. Kholkin, *Solid State Commun.*, 2011, **151**, 536–540.
32 Q. Q. Wang, Z. Wang, X. Q. Liu and X. M. Chen, *J. Am. Ceram. Soc.*, 2012, **95**, 670–675.
33 P. Kumar and M. Kar, *J. Alloys Compd.*, 2014, **584**, 566–572.
34 A. Le Bail, H. Duroy and J. L. Fourquet, *Mater. Res. Bull.*, 1988, **23**, 447–452.
35 J. Rodríguez-Carvajal, *Physica B*, 1993, **192**, 55–69.
36 R. D. Shannon, *Acta Crystallogr., Sect. A: Cryst. Phys., Diffr., Theor. Gen. Crystallogr.*, 1976, **32**, 751–767.
37 A. Palewicz, I. Sosnowska, R. Przenioslo and A. W. Hewat, *Acta Phys. Pol., A*, 2010, **117**, 296–301.
38 D. P. Kozlenko, A. A. Belik, A. V. Belushkin, E. V. Lukin, W. G. Marshall, B. N. Savenko and E. Takayama-Muromachi, *Phys. Rev. B: Condens. Matter Mater. Phys.*, 2011, **84**, 094108.
39 K. Fujii, H. Kato, K. Omoto, M. Yashima, J. Chen and X. Xing, *Phys. Chem. Chem. Phys.*, 2013, **15**, 6779–6782.

40 G. Le Bras, D. Colson, A. Forget, N. Genand-Riondet, R. Tourbot and P. Bonville, *Phys. Rev. B: Condens. Matter Mater. Phys.*, 2009, **80**, 134417.
41 T. Shibata, B. Bunker, J. F. Mitchel and P. Schiffer, *Phys. Rev. Lett.*, 2002, **88**, 207205.
42 L. M. Daniels, R. J. Kashtiban, D. Kepaptsoglou, Q. M. Ramasse, J. Sloan and R. I. Walton, *Chem. – Eur. J.*, 2016, **22**, 18362–18367.
43 C. Ederer and N. A. Spaldin, *Phys. Rev. B: Condens. Matter Mater. Phys.*, 2005, **71**, 060401.
44 C. Weingart, N. Spaldin and E. Bousquet, *Phys. Rev. B: Condens. Matter Mater. Phys.*, 2012, **86**, 094413.
45 S. M. Selbach, M.-A. Einarsrud and T. Grande, *Chem. Mater.*, 2009, **21**, 169–173.
46 J.-T. Han, Y.-H. Huang, X.-J. Wu, C.-L. Wu, W. Wei, B. Peng, W. Huang and J. B. Goodenough, *Adv. Mater.*, 2006, **18**, 2145–2148.
47 R. C. Pullar, *Prog. Mater. Sci.*, 2012, **57**, 1191–1334.
48 D. V. Karpinsky, R. C. Pullar, Y. K. Fetisov, K. E. Kamentsev and A. L. Kholkin, *J. Appl. Phys.*, 2010, **108**, 042012.
49 Z. Huai-Wu and L. Jie, *Ferroelectrics*, 2012, **435**, 13–17.
50 O. Clemens, R. Kruk, E. A. Patterson, C. Loho, C. Reitz, A. J. Wright, K. S. Knight, H. Hahn and P. R. Slater, *Inorg. Chem.*, 2014, **53**, 12572–12583.
51 J. A. Schiemer, R. L. Withers, Y. Liu and M. A. Carpenter, *Chem. Mater.*, 2013, **25**, 4436–4446.
52 V. A. Khomchenko and J. A. Paixão, *J. Mater. Sci.*, 2015, **50**, 7192–7196.
53 V. A. Khomchenko and J. A. Paixão, *J. Phys. D: Appl. Phys.*, 2015, **48**, 345001.
54 V. A. Khomchenko and J. A. Paixão, *Mater. Lett.*, 2016, **169**, 180–184.
55 G. Catalan, J. Seidel, R. Ramesh and J. F. Scott, *Rev. Mod. Phys.*, 2012, **84**, 119–156.
56 V. A. Khomchenko and J. A. Paixão, *Mater. Lett.*, 2016, **183**, 69–72.
57 I. I. Naumov, L. Bellaiche and H. Fu, *Nature*, 2004, **432**, 737–740.
58 J. Mangeri, Y. Espinal, A. Jokisaari, S. P. Alpay, S. Nakhmanson and O. Heinonen, *Nanoscale*, 2017, **9**, 1616–1624.
59 R. D. Johnson, P. A. McClarty, D. D. Khalyavin, P. Manuel, P. Svedlindh and C. S. Knee, *Phys. Rev. B: Condens. Matter Mater. Phys.*, 2017, **95**, 054420.
60 V. A. Khomchenko, L. C. J. Pereira and J. A. Paixão, *J. Appl. Phys.*, 2014, **115**, 164101.
61 S. M. Selbach, T. Tybell, M.-A. Einarsrud and T. Grande, *Chem. Mater.*, 2009, **21**, 5176–5186.